On the mobility of vacancy clusters in reduced activation steels: an atomistic study in the Fe–Cr–W model alloy

2013 J. Phys.: Condens. Matter 25 315401

(http://iopscience.iop.org/0953-8984/25/31/315401)

IOP PUBLISHING JOURNAL OF PHYSICS: CONDENSED MATTER
J. Phys.: Condens. Matter **25** (2013) 315401 (12pp) doi:10.1088/0953-8984/25/31/315401

On the mobility of vacancy clusters in reduced activation steels: an atomistic study in the Fe–Cr–W model alloy

G Bonny[1], N Castin[1], J Bullens[1,2], A Bakaev[1,3], T C P Klaver[4] and D Terentyev[1]

[1] SCK·CEN, Nuclear Materials Science Institute, Boeretang 200, B-2400 Mol, Belgium
[2] Physics Department, Université Libre de Bruxelles, CP 238, Boulevard du Triomphe, B-1050 Bruxelles, Belgium
[3] Center for Molecular Modeling, Ghent University, Technologiepark 903, B-9052 Zwijnaarde, Belgium
[4] Department of Materials Science and Engineering, Delft University of Technology, Mekelweg 2, 2628 CD Delft, The Netherlands

E-mail: gbonny@sckcen.be

Received 6 March 2013, in final form 14 June 2013
Published 10 July 2013
Online at stacks.iop.org/JPhysCM/25/315401

Abstract
Reduced activation steels are considered as structural materials for future fusion reactors. Besides iron and the main alloying element chromium, these steels contain other minor alloying elements, typically tungsten, vanadium and tantalum. In this work we study the impact of chromium and tungsten, being major alloying elements of ferritic Fe–Cr–W-based steels, on the stability and mobility of vacancy defects, typically formed under irradiation in collision cascades. For this purpose, we perform *ab initio* calculations, develop a many-body interatomic potential (EAM formalism) for large-scale calculations, validate the potential and apply it using an atomistic kinetic Monte Carlo method to characterize the lifetime and diffusivity of vacancy clusters. To distinguish the role of Cr and W we perform atomistic kinetic Monte Carlo simulations in Fe–Cr, Fe–W and Fe–Cr–W alloys. Within the limitation of transferability of the potentials it is found that both Cr and W enhance the diffusivity of vacancy clusters, while only W strongly reduces their lifetime. The cluster lifetime reduction increases with W concentration and saturates at about 1–2 at.%. The obtained results imply that W acts as an efficient 'breaker' of small migrating vacancy clusters and therefore the short-term annealing process of cascade debris is modified by the presence of W, even in small concentrations.

(Some figures may appear in colour only in the online journal)

1. Introduction

Due to their creep resistance, high-chromium ferritic–martensitic (F/M) steels are the materials of choice for applications at high temperature and under heavy load. Because of these attractive properties, these steels have caught the attention of the nuclear industry and are candidate materials for fusion and generation IV fission reactors. Besides the main elements in conventional high-Cr martensitic steels, iron, carbon and chromium, such steels also contain several so-called minor alloying elements, such as molybdenum, niobium, vanadium and nickel. For reasons of waste management, however, especially in connection with fusion application, the nuclear materials community focuses on reduced activation derivatives, where some the aforementioned elements are restricted (nickel) and some substituted (molybdenum by tungsten and niobium by tantalum) [1–6].

In this context, a worldwide effort is on-going to study the effect of radiation on structural and functional steels [7].

Radiation is known to degrade the mechanical properties due to the change of micro- and nanostructure caused by the radiation. The change in microstructure is due to the generation and migration of radiation defects and their interaction with the alloying elements and each other. Since many elements enter the steel composition and the steel is exposed to different irradiation conditions, it is a difficult task to identify the role of each element in the degradation process. Regardless of the difficulty, optimization of the steel composition with respect to its in-service properties is a crucial aspect in the assessment of safety and the commercial interests of nuclear plants.

In recent years computer modelling has become a powerful tool to complement the experimental efforts in the rationalization of degradation mechanisms induced by irradiation. The usage of physically-based simulation techniques, being cheap compared to experiments, allows one to rationalize the effects and contributions of specific elements with a desired concentration and space distribution. In the literature, one can find a number of theoretical atomistic studies addressing the effects of chromium and carbon on the microstructural evolution of Fe–Cr steels under irradiation [8–19]. However, the effects of other minor alloying elements, beside Cr, on the properties of radiation defects in ferritic steels have so far not been studied. In this work we focus on the role of tungsten (W), a substitute of molybdenum in conventional F/M steels, and its possible synergy with Cr in the model Fe–Cr–W alloy. Tungsten is an oversized atom in the bcc Fe matrix and acts as solid solution strengthener. It has a rather low solubility limit at elevated temperature (about 1–2 at.%) and beyond it it forms so-called Laves phases. Given that the latter are brittle particles, W is always added to steels in concentrations prohibiting its precipitation.

For our study we use a multi-scale approach and combine density functional theory (DFT) calculations and Monte Carlo techniques to study the stability and mobility of vacancy clusters in random Fe–Cr–W alloys containing up to 2% of dispersed W. Although some calculations are already available in the literature [20], we extend them with new DFT calculations to form a consistent and complete database for fitting and validating an interatomic potential, necessary for the description of radiation defects beyond the DFT scale. With the aid of interatomic potentials, an artificial neural network (ANN) regression to predict the migration barrier for vacancy defects is developed and embedded in an atomistic kinetic Monte Carlo (AKMC) model. The latter is applied to follow the migration path of vacancy clusters of different sizes in Fe–Cr, Fe–W and Fe–Cr–W alloys, and thus to rationalize the role of W and its possible synergy with Cr. As will be shown later, W does not bind strongly with self-interstitial atoms (neither Fe nor Cr), while it exhibits a considerable binding with a vacancy, which increases with the number of W atoms surrounding a vacancy. Hence, we will focus our study on the effect of W on the stability and mobility of small vacancy clusters (<10 defects) that are formed in large numbers directly in collision cascades in pure Fe (see e.g. [21]) as well as in Fe–Cr alloys (see e.g. [22]) at the cooling stage. In addition, these clusters are thermally stable and exhibit considerable mobility. The impact of W on the fate of these vacancy defects is the subject of this paper.

The paper is organized as follows. A short description of the computational methods used (i.e. DFT, interatomic potential formalism and development, details of the ANN-based AKMC) is given in section 2. The results of DFT calculations, fitting of the interatomic potential and derivation of the ANN regression are presented in section 3. AKMC results for the mobility, lifetime and mean free path of the studied vacancy clusters are given in section 4. The paper is finalized with a summary and conclusions.

2. Methods

2.1. Density functional theory calculations

The DFT calculations were performed using the Vienna *ab initio* simulation package (VASP) [23, 24]. VASP is a plane-wave DFT code that implements the Projector Augmented Wave (PAW) method [25, 26]. For reasons of consistency, most settings were taken to be the same as in earlier works [13, 20] to ensure full consistency of the already available and 'to be obtained' data.

Standard PAW potentials supplied with VASP were used with Vosko–Wilk–Nusair parameterization [27] for the local density approximation (LDA) combined with Perdew–Wang [28] parameterization for the generalized gradient approximation (GGA) correction. For Fe, Cr and W potentials, 8, 6 and 6 valence electrons were used, respectively.

Finite-temperature smearing was obtained following the Methfessel–Paxton method with a smearing width of 0.3 eV. The plane-wave cut-off energy was set to 300 eV, which proved sufficient for convergence of the binding and migration energy of the selected configurations. Brillouin zone sampling was performed using the Monkhorst–Pack scheme, where meshes of $3\times3\times3$ k-points proved sufficient for convergence. The total energy was calculated in periodic bcc supercells containing 128 atoms in a fixed volume set to the equilibrium volume of Fe.

For the defect–solute and solute–solute interactions the total binding energy of a configuration containing the objects X_i is defined as,

$$E_b(X_1 \cdots X_n) = \sum_i E(X_i) - \left[E\left(\sum_i X_i \right) + (n-1)E_{\text{ref}} \right], \quad (1)$$

where n is the number of interacting objects, E_{ref} is the energy of the supercell without any objects (bcc Fe), $E(X_i)$ is the energy of the supercell containing the single object X_i, and $E\left(\sum_i X_i\right)$ is the energy of the supercell containing all interacting objects. Within this definition, positive values of E_b denote attraction.

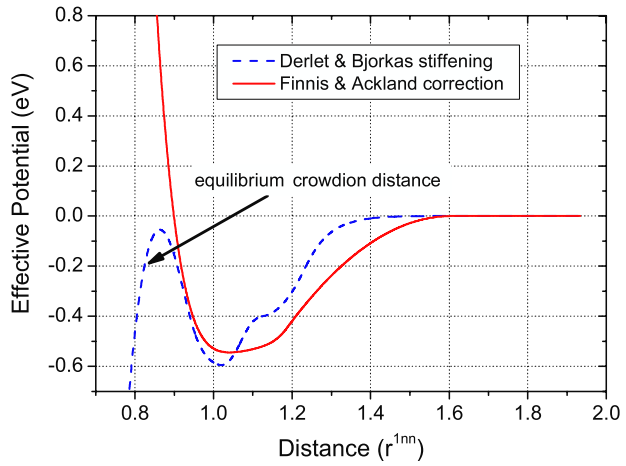

Figure 1. Comparison of the effective pair potentials by Derlet *et al* [37] with stiffening by Björkas *et al* [48], and Finnis and Sinclair [30] with correction by Ackland and Thetford [31].

2.2. Interatomic potentials

In the literature a number of interatomic potentials for bcc W [29–38] and the Fe–Cr system [39–44] are available. Among the Fe–Cr potentials, we only consider those based on the embedded atom method (EAM) which, in addition, can reproduce the inversion in the heat of mixing as predicted by DFT [8, 10–14]. Therefore, three potentials were considered in this work, namely, the two-band model (2BM) potential by Olsson *et al* [42], the concentration dependent model (CDM) by Caro *et al* [43], and the 2BM potential by Bonny *et al* [44]. Historically, both the potentials by Olsson *et al* and Caro *et al* were developed independently of each other at the same time. Although both were fitted to describe radiation damage in the Fe–Cr system, they exhibit some shortcomings, as discussed in [16, 44, 45]. In an effort to overcome the shortcomings of the latter potentials and combine their strong points, the 2BM potential by Bonny *et al* was developed. Since this is the current state-of-the-art, the latter potential is selected in this work.

We note that the Fe-part of the Fe–Cr potential was developed by Mendelev *et al* [46]. The latter potential has been widely used and tested, and as shown in [47] is suitable for studies of radiation damage in Fe.

Consistent with our choice for Fe–Cr, for W too we only consider EAM type potentials. These are the one developed by Finnis and Sinclair [30], with a short-range correction by Ackland and Thetford [31]; and the one developed by Derlet *et al* [37] and stiffened by Björkas *et al* [48]. The latter potential was fitted to recent DFT data and specifically applied to model radiation damage, and is therefore *a priori* preferred. However, when comparing the effective potentials, presented in figure 1, a clear oscillation is present for the latter potential in the equilibrium range (the equilibrium distance between the crowdion is indicated in figure 1), which is not present for the former potential. For simulations in pure W, the latter oscillation is compensated for by the repulsion in the embedding function and, consequently, no artefacts are observed, as shown in [37]. For the purpose of combination with our selected Fe–Cr potential, however, we need the effective form, and such an oscillation can lead to unexpected instabilities for the alloy. For this reason, the potential developed by Finnis and Sinclair with correction by Ackland and Thetford is selected.

To obtain a ternary Fe–Cr–W potential, both Fe–W and Cr–W cross potentials were fitted simultaneously, following the methodology explained in [49]. In short, the fitting can be viewed as a problem of finding the potential parameters that allow one to optimally reproduce a given data set. Mathematically, it can be formulated as the minimization of the overall squared deviation, the so-called objective function, between predicted and reference data. The properties that were explicitly fitted are: the binding energy between W–vacancy, W–W and W–Cr pairs; the W–vacancy migration energy; and the binding energy of both Fe–W and Cr–W mixed ⟨110⟩ dumbbells, all in a bcc Fe matrix. To check the transferability of the potential, many other properties to which the potential is not initially fitted are discussed in section 3. As reference data we use the DFT data set developed in this work. Given the Fe–Cr potential and the W potential in an effective gauge form, the Fe–W and Cr–W interactions fitted in this work are summarized in appendix A.

2.3. Atomistic kinetic Monte Carlo

Atomistic kinetic Monte Carlo methods are widespread tools to study the diffusion-controlled microstructural and micro-chemical evolution of alloys under thermal ageing and irradiation conditions. In these models the evolution of the system is driven by the migration of point defects (here vacancies), whose position is exchanged with nearest neighbour atoms (so called migration jumps). In our model [50], the migration energy is calculated using the nudged elastic band (NEB) method [51] with the IAP as Hamiltonian. As such, the influence of both the chemical environment and the static relaxation is accounted for. The transition frequency, Γ, for an event is determined as,

$$\Gamma = \Gamma_0 \exp\left(\frac{-E_\mathrm{m}}{k_\mathrm{B}T}\right). \tag{2}$$

Here, E_m is the migration energy, k_B is Boltzmann's constant, T is the absolute temperature and Γ_0 is the attempt frequency, in a first approximation taken as a constant, i.e., the Debye frequency of Fe ($\Gamma_0 = 6 \times 10^{12}$ s^{-1}). As NEB calculations of E_m at every simulation step are computationally too costly, we rely on numerical regressions to estimate E_m.

In this work we use artificial neural networks (ANN) as a means of regression [52]. The latter are designed to predict the value of E_m as a function of the local atomic environment. In this work, the exact distribution in space of Fe, Cr and W atoms, as well as vacancies, are accounted for in the local atomic environment. The methodology is extensively described in [50] for the single vacancy, where the assumption of a rigid lattice is particularly sound. In the subsequent work [53] the approach was generalized to vacancy clusters, showing that the rigid lattice assumption remains acceptable even if many vacancies are close to each

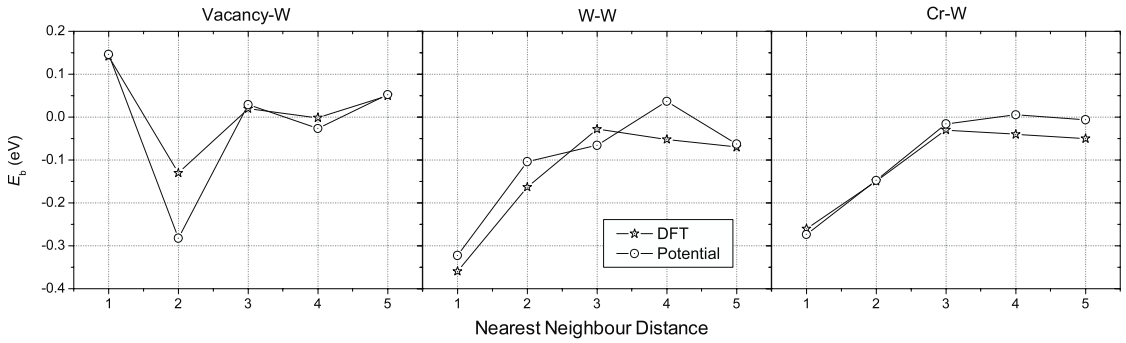

Figure 2. Binding energy between vacancy–W, W–W and Cr–W pairs computed using DFT and the IAP.

other. In the latter paper [53], the methodology we follow to characterize the mobility and stability of vacancy clusters is extensively described. In the following only the essentials are summarized.

Initially, a compact vacancy cluster of predefined size is generated in a box with a prescribed random distribution of solutes. Subsequently, the AKMC simulation is run—thereby following the cluster's centre of gravity—until the cluster dissociates, i.e., at least one vacancy escapes from the cluster (2nn distance criterion). Such simulations are repeated a large number of times (>100) until enough statistics are gathered to calculate the lifetime τ, defined as the average time before dissociation, and the diffusion coefficient D,

$$D = \frac{\langle R^2 \rangle}{6t}. \tag{3}$$

Here $\langle R^2 \rangle$ is the average mean square displacement of the cluster and t the time.

Considering a single vacancy, we also calculated the geometrical correlation factor f_c, which is defined by

$$D = \frac{\Delta^2}{6 \langle t_{1nn} \rangle} f_c. \tag{4}$$

Here, Δ is the 1nn distance, i.e., the distance of an elementary vacancy jump, and $\langle t_{1nn} \rangle$ is the average time increment determined by the mean residence time algorithm [54]. The geometrical correlation factor gives a measure of the randomness of the migration path followed by the vacancy. A value $f_c \approx 1$ means that the diffusion is fully random. A value $f_c \ll 1$, on the other hand, implies that the migration path significantly deviates from a random walk due to either trapping or percolation movement as a result of strong interactions of the vacancy with solute atoms.

3. DFT data set and models validation

The binding energy between vacancy–W, W–W and Cr–W pairs as a function of distance calculated with both DFT and the IAP are presented in figure 2. Focusing on the DFT results first, we observe that the effective interaction range is limited to the first and second nearest neighbour distance. From the figure we observe that both W–W and Cr–W pairs repel each other, while for vacancy–W pairs the sign of the interaction changes, i.e., attraction for 1nn and repulsion for 2nn pairs. As forced during the fit, the potential provides both qualitative and quantitative agreement with the DFT data. However, the vacancy–W repulsion at 2nn distance is overestimated by a factor two.

In table 1 we summarize the binding energy of (i) W–Cr, (ii) W–divacancy, (iii) W–Cr–vacancy, and (iv) interstitial-W complexes, calculated with both DFT and the IAP. For small W–Cr clusters, both methods predict a repulsive interaction for all studied configurations. These results are in line with the repulsive interaction between Cr–Cr [13, 44], W–W and Cr–W pairs (see figure 2).

For W–divacancy configurations, DFT calculations predict the triangular configuration with the divacancy at 2nn as the most stable one. This result can be expected from the W–vacancy pair interactions in figure 2, which predict W–vacancy pairs at 1nn to be the only binding ones and the fact that the divacancy at the 2nn distance is known to be the most stable configuration in bcc Fe [47, 55, 56]. In line with DFT, the same configuration is also predicted as the most stable by the IAP with a similar binding energy. For the less stable configurations, however, the IAP predicts repulsion, in contrast to the DFT data.

For compact W–Cr–vacancy configurations, DFT calculations suggest repulsive interactions for all configurations, except for one that gives neutral interaction. This result is in line with the Cr–W and W–vacancy pair interactions (see figure 2) and the fact that Cr–vacancy pairs have negligible interaction [13, 44]. The latter configuration indeed maximizes the Cr–W distance (thereby minimizing repulsion) and provides the 1nn distance for the W–vacancy pair (thereby maximizing attraction). In line with the DFT data, the order of repulsion is respected by the IAP, although the IAP predicts too strong a repulsion by about a factor two. Since all concern repulsive interactions, the latter is not expected to strongly influence the AKMC simulations.

For the interstitial configurations containing a W atom, the DFT calculations show repulsion for all configurations except for the ⟨110⟩ self interstitial (SIA) and ⟨110⟩ Fe–Cr mixed dumbbell with W in a tensile position. Clearly, W acts as an oversized atom, exhibiting the weakest repulsion, or attraction, at tensile sites. The potential reproduces the latter effect, although the attraction is strongly overestimated. This will probably bias the result of simulations involving SIAs,

Table 1. Binding energy of (i) W–Cr clusters, (ii) W–divacancy, (iii) W–Cr–vacancy and (iv) interstitial-W complexes calculated with both DFT and the IAP. ●—Fe; ⊘—W; ○—Cr; □—vacancy.

Configuration	E_b DFT (eV)	E_b IAP (eV)
(i) 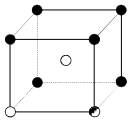	−0.52	−0.62
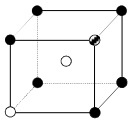	−0.48	−0.52
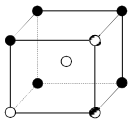	−0.57	−0.99
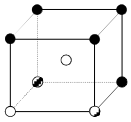	−0.70	−1.08
(ii) 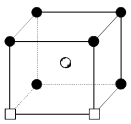	0.39	0.41
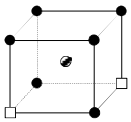	0.31	−0.12
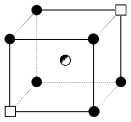	0.16	−0.12
(iii) 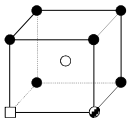	−0.33	−0.59
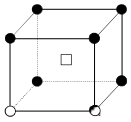	0.01	−0.11
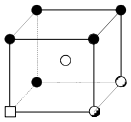	−0.40	−0.91
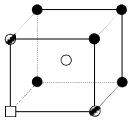	−0.64	−1.25

Table 1. (Continued.)

Configuration	E_b DFT (eV)	E_b IAP (eV)
(iv) 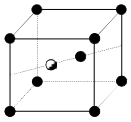	−1.74[a]	−1.97[a]
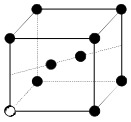	−0.55	−0.98
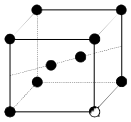	0.05	0.49
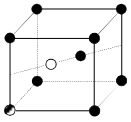	−0.88	−0.46
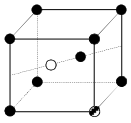	0.10	0.32

[a] Indicates the configuration is included in the fit.

Table 2. Vacancy migration jumps.

Jump	DFT (eV) (forward/back)	Potential (eV) (forward/back)
E_m (Fe)[a]	0.64	0.63
E_m (Cr)[a]	0.57	0.57
E_m (W)[a]	0.72	0.72
E_m (1nn → 2nn)	0.95/0.69	1.01/0.59
E_m (1nn → 3nn)	0.68/0.56	0.45/0.34
E_m (1nn → 5nn)	0.72/0.63	0.64/0.55
E_m (2nn → 4nn)	0.66/0.78	0.65/0.90

[a] Indicates the configurations that are included in the fit.

but will not affect the study of the mobility of vacancy clusters addressed here.

Having discussed the stability of W–Cr point-defect complexes, we now focus on their migration. In table 2 vacancy migration barriers in a bcc Fe matrix with a W atom up to a distance of 5nn—thereby following Le Claire's five-frequency model [57]—calculated by DFT and IAP are presented. For completeness, we also include the values for the Fe self-migration and Cr–vacancy exchange barriers [58]. Firstly, we observe that the W exchange barrier is higher than the Fe-self-diffusion barrier, while for Cr it is the opposite. As forced during the fit, both effects are well reproduced by the IAP. This suggests that local rearrangement of Cr atoms is much faster than for W atoms. With respect to the five-frequency model, the DFT results suggest that all jumps of the vacancy towards the 1nn position with respect to W are favoured—an effect to be expected from the result presented in figure 2—the jump from 3nn to 1nn being the most favourable one. The latter barrier is lower than the self-diffusion barrier in Fe, which suggests the presence of low energy diffusion paths for the vacancy in a dilute Fe–W alloy. All barriers are qualitatively reproduced by the IAP, although the minimum barrier is underestimated by almost a factor two. For our further AKMC simulations,

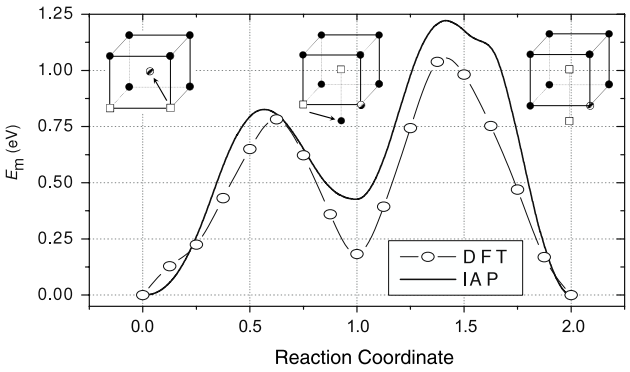

Figure 3. W–divacancy migration barrier calculated from both DFT and the IAP. ●—Fe; ⊘ —W; □—vacancy.

the latter might have an influence on the magnitude of the vacancy (cluster)'s diffusion coefficient, average lifetime and mean free path. However, given the qualitative agreement, no artefacts are expected with respect to the prediction of trends to be derived as a function of Cr and W composition.

The migration path for the most stable W–divacancy complex shown in table 1, calculated by both DFT and the IAP, is shown in figure 3. Migration occurs via a meta-stable state with the divacancy at the 1nn distance. The IAP describes this curve well, both qualitatively and quantitatively.

The quality of the ANN prediction of the migration energy associated with a vacancy jump to a 1nn position in the random Fe–Cr–W system, as calculated with the IAP, is presented in figure 4. The shown examples consist of vacancy clusters containing 1–7 vacancies in a random alloy containing 0–20% Cr and 0–5% W. In the plots the values obtained from the IAP are shown on the abscissa while the ANN predicted values are shown on the ordinate. In this case, perfect agreement represents the bisector in the first quadrant (superposed in the plots). As shown in the figure, the ANN reproduces the vacancy migration barriers very well, with an average error of 38 meV, 45 meV and 65 meV for migrating Fe, Cr and W, respectively. The respective statistical correlation factors are 0.98, 0.97 and 0.97. Given the relatively high complexity of the system, which forces the ANN to account for the effect of four different species that can be differently located on the lattice (Fe, Cr, W and vacancies), the errors induced by the ANN are to be considered fully acceptable.

4. Vacancy cluster mobility

4.1. Binary alloys

Results for pure bcc Fe—studied using the same IAP and methodology—have been already reported in [53]. Those results are taken here as the baseline for comparison with the alloys. Given the technological interest in 9% Cr steels and as a baseline for the ternary Fe–Cr–W alloy, here we focused on the Fe–9Cr alloy.

For all studied binary alloys the obtained results for the single vacancy are shown in figure 5. There, the diffusion coefficient ratio, $R_D = D_{Alloy}/D_{Fe}$, and geometrical correlation factor, f_c, as a function of reciprocal temperature are plotted. For all alloys we observe only a marginal effect on R_D at high temperature; with decreasing temperature, however, R_D increases to about 3 and 4.5 for Fe–9Cr and Fe–2W, respectively at 500 K. At 1% W the effect of W is similar to that of 9% Cr (although less pronounced at low temperature); below 1% W the effect is negligible; and above 1% W it is stronger than in Fe–9Cr.

With respect to the geometrical correlation factor, the effect of Cr is negligible for all temperatures ($f_c \approx 1$), which indicates the randomness of the path followed by the vacancy. In Fe–W, on the other hand, the effect is clearly pronounced: f_c decreases down to 10^{-2}–10^{-3} in the alloys containing 0.1 and 2% W, respectively, at temperatures below 600 K. We also note that the effect on f_c saturates with increasing W content (starting from ∼0.5% W).

The above results can be explained from the DFT and IAP data presented in section 3. For the Fe–9Cr alloy the absence of a correlation is consistent with the negligible interactions between Cr and vacancies at all distances [13]: the path followed by the vacancies remains essentially random in the 9% Cr alloy as in pure Fe ($f_c \approx 1$). The increase in R_D, on the other hand, is probably the consequence of the fact that

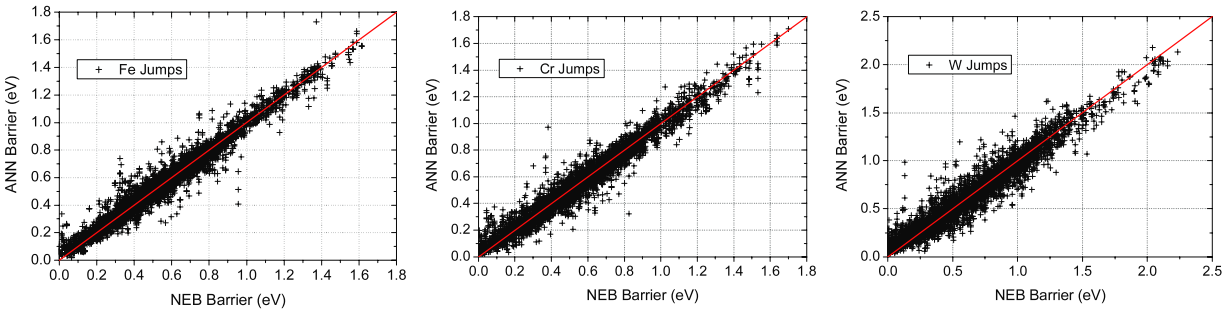

Figure 4. Comparison between NEB calculated and ANN predicted vacancy migration barriers for a migrating Fe atom (left), Cr atom (centre) and W atom (right).

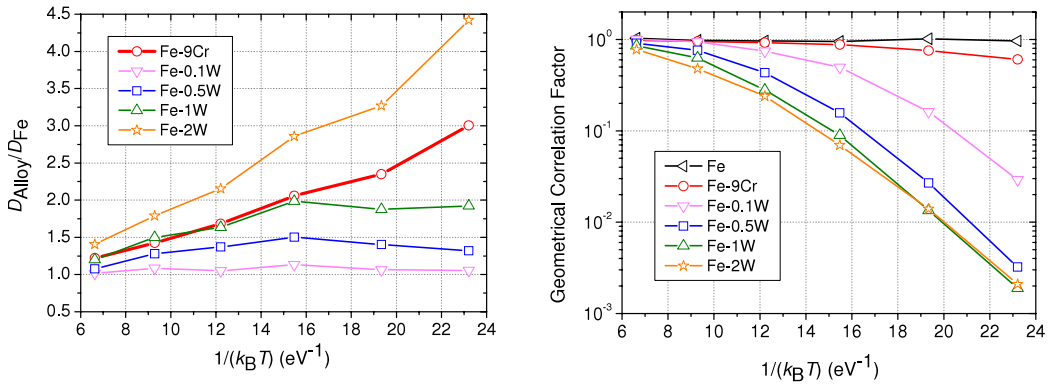

Figure 5. Diffusion coefficient ratio, R_D, and geometrical correlation factor, f_c, for a mono-vacancy as a function of reciprocal temperature $(1/k_BT)$ in binary Fe–9Cr and Fe–W alloys.

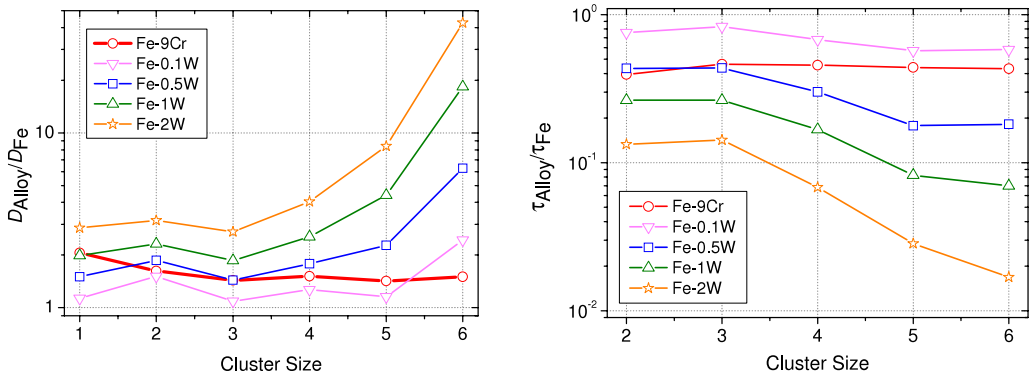

Figure 6. Diffusion coefficient R_D and average lifetime ratio, R_τ, for vacancy clusters as a function of cluster size in binary Fe–9Cr and Fe–W alloys at 750 K.

the exchange migration barrier of Cr in bcc Fe is slightly lower than the self-diffusion barrier in Fe (see table 2), thereby making the overall migration process faster.

The increase of R_D for the Fe–W alloys can be explained by the low energy migration paths found in the five-frequency model by both DFT and the IAP (see section 3) and in connection with the drastic decrease of f_c. The latter indicates strong deviations from the 'random walk' and can be explained by the fact that, because of the strong 1nn neighbour vacancy–W binding energy, most favoured jumps lead the vacancy towards the W atoms, thereby strongly biasing the migration path. Since these jumps have low migration energy, the vacancy can effectively migrate from one W atom to another with, on average, a lower migration energy than in pure Fe. From visualization of the migration path, we observed that the vacancy is indeed often trapped in a low energy migration environment surrounded by a few W atoms, before its random walk continues.

We have calculated R_D and average lifetime ratio, $R_\tau = \tau_{Alloy}/\tau_{Fe}$, for vacancy clusters containing 2–6 vacancies at temperatures between 500 and 1750 K. For completeness and possible future use in object kinetic Monte Carlo simulations, all results are summarized as coefficients of Arrhenius expressions in table B.1, while here we discuss the results obtained at 750 K.

As a representative example, we plot R_D and R_τ as a function of cluster size at 750 K in figure 6. For Fe–9Cr, both R_D and R_τ remain constant for all cluster sizes, increasing and decreasing by a factor of two, respectively. Raising the W content, R_D and R_τ increase and decrease, respectively. The effect of W is as strong as or stronger than the effect of Fe–9Cr starting from about 0.5% W. We also note that the effect of W is most pronounced on R_τ.

For both R_D and R_τ the results can be separated into two groups: clusters containing 1–4 and 5–6 vacancies, respectively. For the first group both ratios remain about constant with cluster size. For the second group R_D increases with cluster size and R_τ remains constant at a lower value.

The combined effect of diffusion coefficient and average cluster lifetime is given by the mean free path ($\delta = \sqrt{6D\tau}$) travelled by the cluster during its lifetime. The ratio of the latter, $R_\delta = \delta_{Alloy}/\delta_{Fe}$, between the alloy and pure Fe at 750 K is plotted in figure 7. We observe that at constant cluster size R_δ reduces with increasing W content, with an effect as strong as or stronger than Fe–9Cr starting from about 0.5% W. For Fe–9Cr, R_δ remains constant with cluster size, while for W the latter first decreases and then increases with cluster size, with a minimum for a size of five. We also observe that R_δ decreases with increasing W content.

4.2. Ternary alloys

For all studied ternary alloys the obtained results for the single vacancy are shown in figure 8. There, the diffusion coefficient

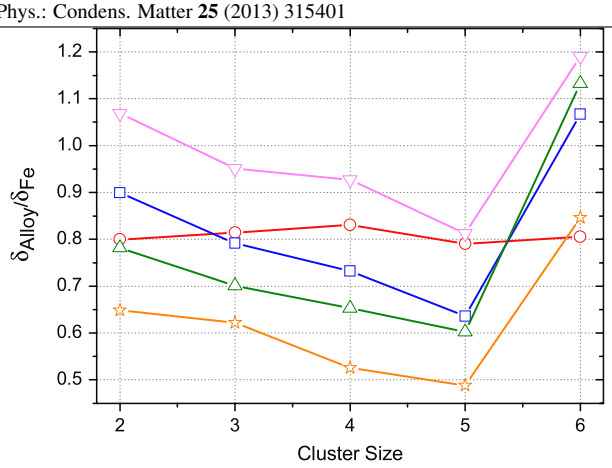

Figure 7. Mean free path ratio, R_δ, for vacancy clusters as a function of cluster size in binary Fe–9Cr and Fe–W alloys at 750 K.

ratio, $R_D = D_{Alloy}/D_{Fe}$, and geometrical correlation factor, f_c, as a function of reciprocal temperature, $1/k_BT$, are plotted. Qualitatively, the results follow the trends of the binary Fe–W alloys. Quantitatively, the combined effect of W and Cr does not significantly modify f_c (compared to binary Fe–W) but further increases R_D (compared to Fe–9Cr).

For vacancy clusters, we have calculated R_D and R_τ for vacancy clusters containing 2–6 vacancies at temperatures between 500 and 1750 K. As for the binary alloys, all results are summarized as coefficients of Arrhenius expressions in table B.1.

As a representative example, we plotted R_D and R_τ as a function of cluster size at 750 K in figure 9. The same trends are followed as in the binary case. Compared to the Fe–9Cr case, R_D and R_τ are further increased and decreased, respectively.

The combined effect of W and Cr on the mean free path ratio, R_δ, at 750 K is shown in figure 10. As for R_D and R_τ, R_δ behaves similarly to the binary.

To reveal the synergy between Cr and W we compare the ratio of the diffusion coefficient ratio for the ternary alloy with the product of the ratios for the Fe–9Cr and Fe–W alloys, $R_D^{Fe-9Cr-W}/(R_D^{Fe-9Cr}R_D^{Fe-W})$. The latter ratio is plotted in figure 11 as a function of composition for all studied cluster sizes. The ratio varies between 0.4 and 1.5, which indicates that no significant synergy exist between Cr and W in the studied composition range for the studied cluster sizes.

5. Summary and conclusive remarks

We performed a multi-scale study addressing the mobility and lifetime of vacancy clusters in bcc Fe–Cr, Fe–W and Fe–Cr–W alloys. We performed DFT calculations and used

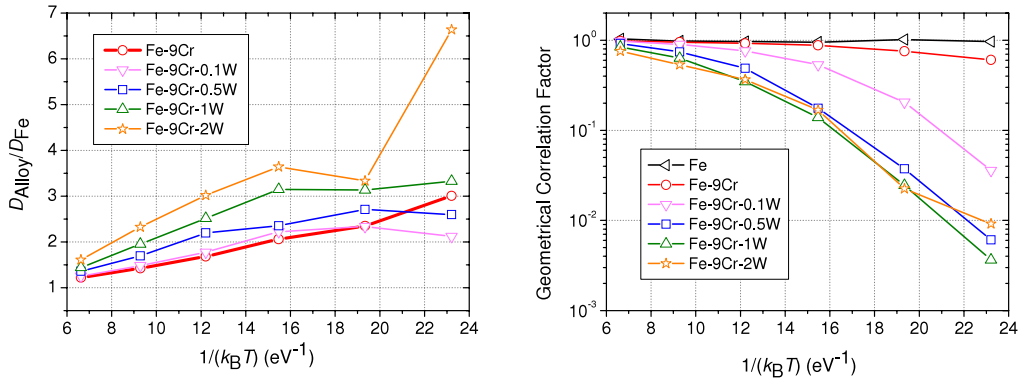

Figure 8. Diffusion coefficient ratio, R_D, and geometrical correlation factor, f_c, for a mono-vacancy as a function of reciprocal temperature ($1/k_BT$) in binary Fe–9Cr and ternary Fe–9Cr–W alloys.

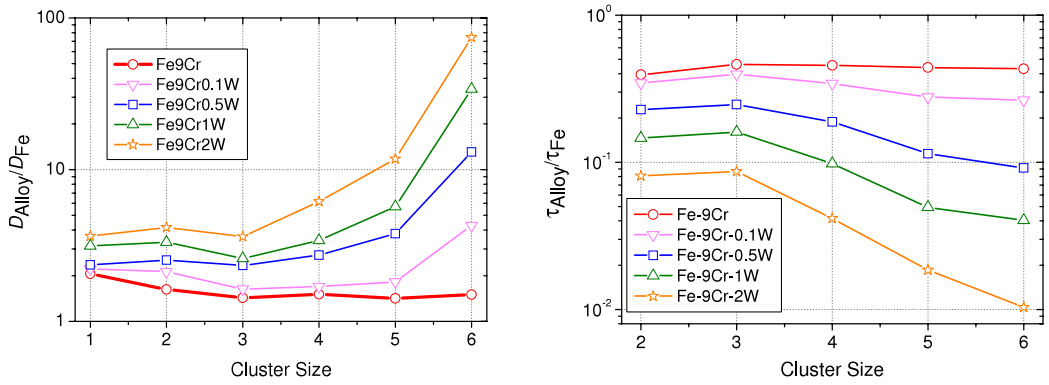

Figure 9. Diffusion coefficient ratio, R_D, and average lifetime ratio, R_τ, for vacancy clusters as a function of cluster size in binary Fe–9Cr and ternary Fe–9Cr–W alloys at 750 K.

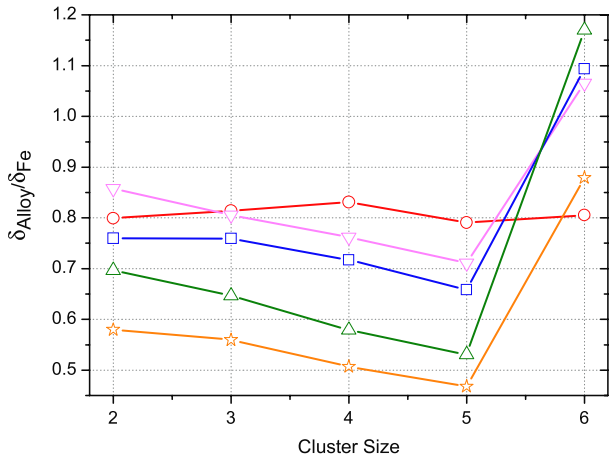

Figure 10. Mean free path ratio, R_δ, for vacancy clusters as a function of cluster size in binary Fe–9Cr and ternary Fe–9Cr–W alloys at 750 K.

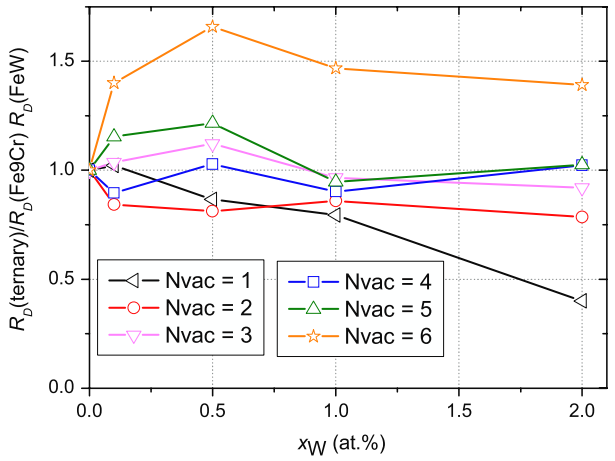

Figure 11. Comparison of the ratio of the diffusion coefficient ratio for the ternary alloy with the product of the ratios for the Fe–9Cr and Fe–W alloys, $R_D^{\text{Fe–9Cr–W}}/(R_D^{\text{Fe–9Cr}}R_D^{\text{Fe–W}})$, as a function of W composition for clusters containing 1–6 vacancies.

them to fit and validate the developed IAP. In turn, the latter was used to derive an ANN regression to predict the migration barrier of vacancies as a function of local atomic environment in bcc Fe–Cr–W alloys. Based on the obtained regression, AKMC simulations were executed to characterize the mobility, lifetime and free path (until the break event) of small vacancy clusters (containing up to six vacancies), known to be as mobile as a single vacancy. As a result, we provide the database of the properties of small vacancy clusters to be applied in rate theory or object kinetic Monte Carlo (OKMC) models.

From the DFT data we conclude that W is a slow diffuser and Cr a fast diffuser compared to Fe. We also conclude that fast vacancy migration paths exist in dilute Fe–Cr and Fe–W alloys.

The developed IAP provides good qualitative agreement with the DFT data, although it was only fitted to a limited number of configurations. Therefore the IAP provides good transferability and can be used in other atomistic studies, e.g., molecular dynamics studies in the Fe–Cr–W system. As also mentioned in [44], we emphasize that the present potential was fitted to the ferro-magnetic alloy and its application should be limited to temperatures well below the Curie temperature.

The ANN regression trained on random examples of vacancy migration barriers in the ternary alloy using the IAP proves an accurate and fast method for on-the-fly migration barrier calculations.

Within the limitation of transferability of the fitted potentials, the AKMC results show that for a single vacancy the addition of W or Cr enhances diffusivity by a factor of 2–4. The increase of 9%Cr is equivalent to that of Fe–(1–2)W. The enhancement of diffusivity is due to Cr–vacancy exchange (occurring with a lower energy barrier), since the geometric correlation factor indicates no correlated movement. For Fe–W, on the other hand, the enhanced diffusion is due to some correlated movement.

For vacancy clusters, the amplification of cluster diffusivity increases for larger vacancy clusters (starting from size four). At the same time, the lifetime monotonically decreases with W concentration. The larger the cluster size, the larger the decrease of the lifetime is. We note that in Fe–9Cr, both the lifetime decrease and diffusivity enhancement do not depend on the size of a vacancy cluster. For the ternary alloy, no synergetic effects are observed, and the alloy behaves as the superposition of the Fe–9Cr and Fe–W alloys. We also note that W atoms remain immobile in all simulations and solely act as ‘break up’ centres for vacancy clusters.

We conclude that the presence of W in concentrations of 1–2% has a huge impact on the stability of migrating vacancy clusters, i.e., they do breakup as soon as a W atom is met. This result implies that W should effectively suppress the growth of in-cascade-formed vacancy clusters. Hence, we conclude that one of the effects of W in the microstructural evolution under irradiation is to suppress the nucleation of stable vacancy clusters, which may grow into voids. The validity of the latter statement is to be validated using object kinetic Monte Carlo simulations in our future work.

Acknowledgments

This work, supported by the European Commission under the Contract of Association between EURATOM/SCK•CEN, was carried out within the framework of the European Fusion Development Agreement. Part of the calculations have been performed at HPC Julich within the ‘EMACS’ project. A part of this work was carried out using the HELIOS supercomputer system at Computational Simulation Centre of International Fusion Energy Research Centre (IFERC-CSC), Aomori, Japan, under the Broader Approach collaboration between Euratom and Japan, implemented by Fusion for Energy and JAEA.

Appendix A. Interatomic potential parameterization

The Fe–Cr 2BM potential is taken as defined in [44]. For W, the EAM potential functions V, ϕ and F, representing

Table A.1. Fit parameters in equation (A.2) defining the cross pair interactions.

	V_{FeW}		V_{CrW}	
i	r_i (Å)	a_i (Å)	r_i (Å)	a_i (Å)
1	2.000 000 00	$2.506\,120\,80 \times 10^{2}$	2.000 000 00	$-5.901\,333\,72 \times 10^{1}$
2	2.372 500 00	$1.526\,516\,53 \times 10^{0}$	2.428 571 43	$2.074\,845\,11 \times 10^{1}$
3	2.745 000 00	$1.317\,206\,31 \times 10^{1}$	2.857 142 86	$4.323\,095\,50 \times 10^{0}$
4	3.117 500 00	$-1.418\,631\,85 \times 10^{0}$	3.285 714 29	$-5.914\,255\,08 \times 10^{-1}$
5	3.490 000 00	$7.377\,903\,06 \times 10^{-1}$	3.714 285 71	$1.201\,928\,24 \times 10^{0}$
6	3.862 500 00	$8.183\,511\,52 \times 10^{-1}$	4.142 857 14	$-4.465\,498\,39 \times 10^{-1}$
7	4.235 000 00	$-9.977\,725\,91 \times 10^{-1}$	4.571 428 57	$1.836\,742\,21 \times 10^{-2}$
8	4.607 500 00	$4.667\,754\,72 \times 10^{-1}$	5.000 000 00	$-2.431\,542\,14 \times 10^{-2}$
9	4.980 000 00	$-1.439\,188\,05 \times 10^{-1}$		

the (repulsive) pair potential, density function and embedding function, respectively, are provided in [30] and corrected in [31]. For reasons of compatibility with the Fe–Cr and below-defined cross potentials, the latter functions undergo the gauge transformation [30, 59],

$$\begin{aligned} V_{\mathrm{eff}}(r) &= V(r) - 2C\phi(r) \\ \phi_{\mathrm{eff}}(r) &= S\phi(r) \\ F_{\mathrm{eff}}(\rho) &= F\left(\frac{\rho}{S}\right) + \frac{C}{S}\rho, \end{aligned} \tag{A.1}$$

with $C = 1.698\,285\,950 \times 10^{-1}$ and $S = 2.405\,998\,560 \times 10^{-2}$. The latter functions V_{eff}, ϕ_{eff} and F_{eff} must be used in combination with the Fe–Cr and cross potentials determined in the following.

The cross pair potentials V_{FeW} and V_{CrW} are parameterized by the cubic spline expansion,

$$V(r) = \sum_{i=1}^{N_{\mathrm{p}}} a_i (r_i - r)^3 \, H(r_i - r), \tag{A.2}$$

where N_{p} denotes the number of knots, r_i are the knots, a_i are the fitting parameters and H denotes the Heaviside unit step function. The optimized parameters for V_{FeW} and V_{CrW} are shown in table A.1.

Appendix B. Diffusion coefficients and lifetime

We have performed simulations to parameterize the diffusion coefficient, D, and lifetime, τ, of vacancy clusters of size 1–6 in the temperature range 500–1750 K for Fe, Fe–Cr, Fe–W and Fe–Cr–W alloys. For convenience and easy extrapolation the results are tabulated as coefficients for the following Arrhenius expressions,

$$D = D_0 \exp\left(\frac{-E_{\mathrm{m}}}{k_{\mathrm{B}}T}\right), \tag{B.1}$$

$$\tau = \tau_0 \exp\left(\frac{E_{\mathrm{diss}}}{k_{\mathrm{B}}T}\right). \tag{B.2}$$

Here D_0 and τ_0 are pre-factors and E_{m} and E_{diss} are the migration and dissociation energy, respectively. For all studied

Table B.1. Summary of the Arrhenius coefficients for the diffusion coefficient and lifetime for all studied alloys and vacancy cluster sizes.

N_{vac}	x_{Cr} (at.%)	x_{W} (at.%)	D_0 (m^2 s^{-1})	E_{m} (eV)	τ_0 (s)	E_{diss} (eV)
1	0.0	0.0	4.93×10^{-7}	0.649		
	0.0	0.1	5.15×10^{-7}	0.647		
	0.0	0.5	5.57×10^{-7}	0.638		
	0.0	1.0	5.59×10^{-7}	0.622		
	0.0	2.0	4.66×10^{-7}	0.582		
	9.0	0.0	4.29×10^{-7}	0.596		
	9.0	0.1	5.43×10^{-7}	0.614		
	9.0	0.5	5.87×10^{-7}	0.610		
	9.0	1.0	6.11×10^{-7}	0.600		
	9.0	2.0	5.52×10^{-7}	0.577		
2	0.0	0.0	3.92×10^{-7}	0.652	2.37×10^{-14}	0.819
	0.0	0.1	4.78×10^{-7}	0.638	2.97×10^{-14}	0.786
	0.0	0.5	4.83×10^{-7}	0.625	4.64×10^{-14}	0.721
	0.0	1.0	1.90×10^{-7}	0.550	6.37×10^{-14}	0.669
	0.0	2.0	2.04×10^{-7}	0.535	7.07×10^{-14}	0.618
	9.0	0.0	3.13×10^{-7}	0.604	3.84×10^{-14}	0.728
	9.0	0.1	4.52×10^{-7}	0.612	4.08×10^{-14}	0.715
	9.0	0.5	4.35×10^{-7}	0.598	5.26×10^{-14}	0.672
	9.0	1.0	4.58×10^{-7}	0.584	6.60×10^{-14}	0.628
	9.0	2.0	3.04×10^{-7}	0.543	6.98×10^{-14}	0.587

Table B.1. (Continued.)

N_{vac}	x_{Cr} (at.%)	x_W (at.%)	D_0 (m^2 s^{-1})	E_m (eV)	τ_0 (s)	E_{diss} (eV)
3	0.0	0.0	1.07×10^{-7}	0.552	3.10×10^{-14}	0.762
	0.0	0.1	8.37×10^{-8}	0.530	3.57×10^{-14}	0.741
	0.0	0.5	7.36×10^{-8}	0.504	5.58×10^{-14}	0.670
	0.0	1.0	7.68×10^{-8}	0.490	6.93×10^{-14}	0.624
	0.0	2.0	7.67×10^{-8}	0.465	8.13×10^{-14}	0.573
	9.0	0.0	1.07×10^{-7}	0.528	3.97×10^{-14}	0.696
	9.0	0.1	9.33×10^{-8}	0.511	4.41×10^{-14}	0.679
	9.0	0.5	1.78×10^{-7}	0.530	5.71×10^{-14}	0.632
	9.0	1.0	8.70×10^{-8}	0.476	6.46×10^{-14}	0.596
	9.0	2.0	7.47×10^{-8}	0.445	7.59×10^{-14}	0.546
4	0.0	0.0	1.07×10^{-7}	0.610	6.55×10^{-15}	0.950
	0.0	0.1	1.55×10^{-7}	0.618	1.14×10^{-14}	0.890
	0.0	0.5	7.23×10^{-8}	0.547	2.34×10^{-14}	0.790
	0.0	1.0	5.71×10^{-8}	0.509	2.89×10^{-14}	0.739
	0.0	2.0	5.52×10^{-8}	0.477	4.17×10^{-14}	0.657
	9.0	0.0	1.20×10^{-7}	0.591	9.12×10^{-15}	0.878
	9.0	0.1	9.91×10^{-8}	0.571	1.24×10^{-14}	0.840
	9.0	0.5	6.95×10^{-8}	0.517	2.03×10^{-14}	0.770
	9.0	1.0	6.82×10^{-8}	0.501	2.88×10^{-14}	0.705
	9.0	2.0	6.56×10^{-8}	0.461	3.87×10^{-14}	0.630
5	0.0	0.0	2.69×10^{-7}	0.775	1.33×10^{-15}	1.198
	0.0	0.1	2.28×10^{-7}	0.755	2.71×10^{-15}	1.116
	0.0	0.5	1.36×10^{-7}	0.678	8.86×10^{-15}	0.964
	0.0	1.0	9.41×10^{-8}	0.612	1.19×10^{-14}	0.895
	0.0	2.0	7.77×10^{-8}	0.558	1.61×10^{-14}	0.807
	9.0	0.0	2.83×10^{-7}	0.758	1.77×10^{-15}	1.128
	9.0	0.1	2.16×10^{-7}	0.722	3.63×10^{-15}	1.050
	9.0	0.5	1.16×10^{-7}	0.635	7.68×10^{-15}	0.945
	9.0	1.0	8.10×10^{-8}	0.585	1.20×10^{-14}	0.862
	9.0	2.0	8.50×10^{-8}	0.541	1.49×10^{-14}	0.784
6	0.0	0.0	1.27×10^{-6}	1.037	3.01×10^{-16}	1.474
	0.0	0.1	4.23×10^{-7}	0.909	5.25×10^{-16}	1.403
	0.0	0.5	3.39×10^{-7}	0.833	1.27×10^{-15}	1.271
	0.0	1.0	1.00×10^{-7}	0.685	1.76×10^{-15}	1.188
	0.0	2.0	7.24×10^{-8}	0.610	3.81×10^{-15}	1.046
	9.0	0.0	1.53×10^{-6}	1.035	3.46×10^{-16}	1.414
	9.0	0.1	3.20×10^{-7}	0.854	7.81×10^{-16}	1.326
	9.0	0.5	1.53×10^{-7}	0.734	1.53×10^{-15}	1.214
	9.0	1.0	7.53×10^{-8}	0.627	1.96×10^{-15}	1.146
	9.0	2.0	5.32×10^{-8}	0.554	2.98×10^{-15}	1.030

alloy compositions and vacancy cluster sizes these parameters are given in table B.1. We note that the temperature range 500–1750 K was chosen as a compromise between the number of points for the Arrhenius plot and computation time. As the potential represents the ferro-magnetic alloy, all extracted data (see table B.1) must be interpreted as data for the ferro-magnetic alloy.

References

[1] Klueh R L and Bloom E E 1985 *Nucl. Eng. Des./Fusion* **2** 383
[2] Dulieu D, Tupholme K W and Butterworth G J 1986 *J. Nucl. Mater.* **141–143** 1097
[3] Tamura M, Hayakawa H, Tanimura M, Hishinuma A and Kondo T J 1986 *J. Nucl. Mater.* **141–143** 1067
[4] Noda T, Abe F, Araki H and Okada M 1986 *J. Nucl. Mater.* **141–143** 1102
[5] Klueh R L, Gelles D S and Lechtenberg T A 1986 *J. Nucl. Mater.* **141–143** 1081
[6] Gelles D S, Hsu C Y and Lechtenberg T A 1988 *J. Nucl. Mater.* **155–157** 902
[7] Fazio C, Alamo A, Almazouzi A, De Grandis S, Gomez-Briceno D, Henry J, Malerba L and Rieth M 2009 *J. Nucl. Mater.* **392** 316
[8] Olsson P, Abrikosov I A, Vitos L and Wallenius J 2003 *J. Nucl. Mater.* **321** 84
[9] Mirzoev A A, Yalalov M M and Mirzaev D A 2004 *Phys. Met. Metallogr.* **97** 336
[10] Klaver T P C, Drautz R and Finnis M W 2006 *Phys. Rev.* B **74** 094435
[11] Olsson P, Abrikosov I A and Wallenius J 2006 *Phys. Rev.* B **73** 104416
[12] Nguyen-Mahn D, Lavrentiev M Yu and Dudarev S L 2007 *J. Comput. Aided Mater. Des.* **14** 159
[13] Olsson P, Domain C and Wallenius J 2007 *Phys. Rev.* B **75** 014110
[14] Erhart P, Sadigh B and Caro A 2008 *Appl. Phys. Lett.* **92** 141904
[15] Klaver T P C, Olsson P and Finnis M W 2007 *Phys. Rev.* B **76** 214110

[16] Klaver T P C, Bonny G, Olsson P and Terentyev D 2010 *Modelling Simul. Mater. Sci. Eng.* **18** 075004
[17] Johnson R 1965 *Acta Metall.* **13** 1259
[18] Domain C, Becquart C and Foct J 2004 *Phys. Rev.* B **69** 144112
[19] Terentyev D, Bonny G, Bakaev A and Van Neck D 2012 *J. Phys.: Condens. Matter* **24** 385401
[20] Olsson P, Klaver T P C and Domain C 2010 *Phys. Rev.* B **81** 054102
[21] Bacon D J, Gao F and Osetsky Yu N 2000 *J. Nucl. Mater.* **276** 1
[22] Terentyev D *et al* 2006 *J. Nucl. Mater.* **349** 119
[23] Kresse G and Hafner J 1993 *Phys. Rev.* B **47** RC558
[24] Kresse G and Furthmuller J 1996 *Phys. Rev.* B **54** 11169
[25] Blöchl P E 1994 *Phys. Rev.* B **50** 17953
[26] Kresse G and Joubert D 1999 *Phys. Rev.* B **59** 1758
[27] Vosko S H, Wilk L and Nusair M 1980 *Can. J. Phys.* **58** 1200
[28] Perdew J P, Chevary J A, Vosko S H, Jackson K A, Pederson M R, Singh D J and Fiolhais C 1992 *Phys. Rev.* B **46** 6671
[29] Johnson R A 1983 *Phys. Rev.* B **27** 2014
[30] Finnis M W and Sinclair J E 1984 *Phil. Mag.* A **50** 45
[31] Ackland G J and Thetford R 1987 *Phil. Mag.* A **56** 15
[32] Johnson R A and Oh D J 1989 *J. Mater. Res.* **4** 1195
[33] Baskes M I 1992 *Phys. Rev.* B **46** 2727
[34] Foiles S M 1993 *Phys. Rev.* B **48** 4287
[35] Lee B-J, Baskes M I, Kim H and Cho Y K 2001 *Phys. Rev.* B **64** 184102
[36] Juslin N, Erhart P, Träskelin P, Nord J, Henriksson K O E, Nordlund K, Salonen E and Albe K 2005 *J. Appl. Phys.* **98** 123520
[37] Derlet P M, Nguyen-Manh D and Dudarev S L 2007 *Phys. Rev.* B **76** 054107
[38] Mrovec M, Gröger R, Bailey A G, Nguyen-Manh D, Elsässer C and Vitek V 2007 *Phys. Rev.* B **75** 104119
[39] Shim J-H, Lee H-J and Wirth B D 2006 *J. Nucl. Mater.* **351** 56
[40] Wallenius J, Olsson P, Lagerstedt C, Sandberg N, Chakarova R and Pontikis V 2004 *Phys. Rev.* B **69** 094103
[41] Stukowski A, Sadigh B, Erhart P and Caro A 2009 *Modelling Simul. Mater. Sci. Eng.* **17** 075005
[42] Olsson P, Wallenius J, Domain C, Nordlund K and Malerba L 2005 *Phys. Rev.* B **72** 214119
Olsson P, Wallenius J, Domain C, Nordlund K and Malerba L 2006 *Phys. Rev.* B **74** 1 (erratum)
[43] Caro A, Crowson D A and Caro M 2005 *Phys. Rev. Lett.* **95** 075702
[44] Bonny G, Pasianot R C, Terentyev D and Malerba L 2011 *Phil. Mag.* **91** 1724
[45] Terentyev D, Bonny G, Castin N, Domain C, Malerba L, Olsson P, Moloddtsov V and Pasianot R C 2011 *J. Nucl. Mater.* **409** 167
[46] Mendelev M I, Han S, Srolovitz D J, Ackland G J, Sun D Y and Asta M 2003 *Phil. Mag.* **83** 3977
[47] Malerba L *et al* 2010 *J. Nucl. Mater.* **406** 19
[48] Björkas C, Nordlund K and Dudarev S 2009 *Nucl. Instrum. Methods Phys. Res.* B **267** 3204
Björkas C, Nordlund K and Dudarev S 2010 *Nucl. Instrum. Methods Phys. Res.* B **268** 1529 (erratum)
[49] Bonny G, Pasianot R C and Malerba L 2009 *Phil. Mag.* **89** 3451
[50] Castin N and Malerba L 2010 *J. Chem. Phys.* **132** 074507
[51] Henkelman G and Jónsson H 2000 *J. Chem. Phys.* **113** 9901
[52] Bishop C M 1995 *Neural Networks for Pattern Recognition* (Oxford: Clarendon)
[53] Castin N, Pascuet M I and Malerba L 2012 *J. Nucl. Mater.* **429** 315
[54] Young W M and Elcock E W 1966 *Proc. Phys. Soc. Lond.* **89** 735
[55] Domain C and Becquart C S 2001 *Phys. Rev.* B **65** 024103
[56] Becquart C S and Domain C 2003 *Nucl. Instrum. Methods Phys. Res.* B **202** 44
[57] Le Claire A D 1970 *Physical Chemistry: An Advanced Treatise* vol 10, ed H Eyring (New York: Academic) chapter 5
[58] Nguyen-Manh D, Lavrentiev M Yu and Dudarev S L 2008 *C. R. Phys.* **9** 379
[59] Bonny G and Pasianot R C 2010 *Phil. Mag. Lett.* **90** 559